

Physics prospects of future neutrino oscillation experiments in Asia

Kaoru Hagiwara ^a

^aTheory Division, KEK, Tsukuba 305-0801 Japan

The three neutrino model has 9 physical parameters, 3 neutrino masses, 3 mixing angles and 3 CP violating phases. Among them, neutrino oscillation experiments can probe 6 parameters: 2 mass squared differences, 3 mixing angles, and 1 CP phase. The experiments performed so far determined the magnitudes of the two mass squared differences, the sign of the smaller mass squared difference, the magnitudes of two of the three mixing angles, and the upper bound on the third mixing angle. The sign of the larger mass squared difference (the neutrino mass hierarchy pattern), the magnitude of the third mixing angle and the CP violating phase, and a two-fold ambiguity in the mixing angle that dictates the atmospheric neutrino oscillation should be determined by future oscillation experiments. In this talk, I introduce a few ideas of future long baseline neutrino oscillation experiments which make use of the super neutrino beams from J-PARC (Japan Proton Accelerator Research Complex) in Tokai village. We examine the potential of HyperKamiokande (HK), the proposed 1 Mega-ton water Čerenkov detector, and then study the fate and possible detection of the off-axis beam from J-PARC in Korea, which is available free throughout the period of the T2K (Tokai-to-SuperKamiokande) and the possible T-to-HK projects. Although the CP violating phase can be measured accurately by studying $\nu_\mu \rightarrow \nu_e$ and $\bar{\nu}_\mu \rightarrow \bar{\nu}_e$ oscillations at HK, there appear multiple solution ambiguities which can be solved only by determining the neutrino mass hierarchy and the twofold ambiguity in the mixing angle. We show that very long baseline experiments with higher energy beams from J-PARC and a possible huge Water Čerenkov Calorimeter detector proposed in Beijing can resolve the neutrino mass hierarchy. If such a detector can be built in China, future experiments with a muon storage ring neutrino factory at J-PARC will be able to lift all the degeneracies in the three neutrino model parameters.

1. Introduction

All the experimental observations on neutrino physics, with a notable exception of the LSND experiment [1], can be accommodated well in the three neutrino model. The atmospheric neutrino oscillation first observed by Super-Kamiokande in 1998 [2] and the observed deficit of the muon neutrino flux in the K2K experiment [3] can be interpreted as $\nu_\mu \rightarrow \nu_\tau$ oscillation with the 90% CL allowed ranges [4]

$$1.9 \times 10^{-3} < \delta m_{\text{ATM}}^2 (\text{eV}^2) < 3.0 \times 10^{-3}, \\ \sin^2 2\theta_{\text{ATM}} > 0.90. \quad (1)$$

The observed deficits of the solar neutrinos [5] and the reactor anti-neutrinos by the KamLand experiment can be interpreted as $\nu_e \rightarrow \nu_\mu$ or ν_τ oscillation with [6]

$$\delta m_{\text{SOL}}^2 = 8.2_{-0.5}^{+0.6} \times 10^{-5} \text{eV}^2,$$

$$\tan^2 \theta_{\text{SOL}} = 0.40_{-0.07}^{+0.09}. \quad (2)$$

No observation of the deficit of the reactor $\bar{\nu}_e$ flux constrains the third mixing angle [7]

$$\begin{aligned} \sin^2 2\theta_{\text{RCT}} &< 0.20 \text{ for } \delta m^2 = 2.0 \times 10^{-3} \text{eV}^2, \\ \sin^2 2\theta_{\text{RCT}} &< 0.16 \text{ for } \delta m^2 = 2.5 \times 10^{-3} \text{eV}^2, \\ \sin^2 2\theta_{\text{RCT}} &< 0.14 \text{ for } \delta m^2 = 3.0 \times 10^{-3} \text{eV}^2, \end{aligned} \quad (3)$$

at the 90% CL. Since the magnitude of the mass squared difference of order 1 eV² associated with the $\nu_\mu \rightarrow \nu_e$ oscillation observed by the LSND experiment is much bigger than those of the above differences, once their finding is confirmed by the MiniBoone experiment [8], we need at least one more neutrinos. Nevertheless, I would like to discuss physics prospects of future neutrino oscillation experiments in the framework of the three neutrino model, mainly because of my prejudice that I find no compelling theoretical reason for

the existence of more than three light neutrinos. Therefore, once the LSND observation is confirmed by MiniBoone, we should revise all our thoughts from scratch.

In the three neutrino model, the three weak interaction eigenstates ν_α ($\alpha = e, \mu, \tau$) that appear in the universal charged current interactions and the three mass eigenstates ν_i ($i = 1, 2, 3$) are related by the 3×3 MNS (Maki-Nakagawa-Sakata) matrix [9]

$$\nu_\alpha = \sum_{i=1}^3 (V_{\text{MNS}})_{\alpha i} \nu_i. \quad (4)$$

The MNS matrix can be expressed as [5]

$$V_{\text{MNS}} = U \mathcal{P} = U \text{diag}(e^{i\alpha_1/2}, e^{i\alpha_2/2}, 1) \quad (5)$$

with the two Majorana phases α_1 and α_2 . The 3×3 unitary matrix U can be parameterized in terms of the three angles and one CP violating phase just like the CKM matrix:

$$U = O_{23} P_\delta O_{13} P_\delta^\dagger O_{12} \\ = \begin{pmatrix} U_{e1} & U_{e2} & U_{e3} \\ U_{\mu 1} & U_{\mu 2} & U_{\mu 3} \\ U_{\tau 1} & U_{\tau 2} & U_{\tau 3} \end{pmatrix}, \quad (6)$$

where O_{ij} are the orthogonal rotation matrix in the ij plane, and $P_\delta = \text{diag}(1, 1, e^{i\delta})$ gives the CP violating phase of the MNS matrix $\delta = \delta_{\text{MNS}}$. Because the present neutrino oscillation experiments constrain directly the three elements,

$$U_{e3} = s_{13} e^{-i\delta}, \quad (7a)$$

$$U_{e2} = s_{12} c_{13}, \quad (7b)$$

$$U_{\mu 3} = s_{23} c_{13}, \quad (7c)$$

we find it most convenient to adopt the convention [10] where these three matrix elements in the upper-right corner of the U matrix are chosen as the independent parameters. The phase convention of Refs. [10,11]

$$U_{e3} = |U_{e3}| e^{-i\delta}, \quad (8a)$$

$$U_{e1} \geq U_{e2} \geq 0, \quad (8b)$$

$$U_{\mu 3}, U_{\tau 3} \geq 0, \quad (8c)$$

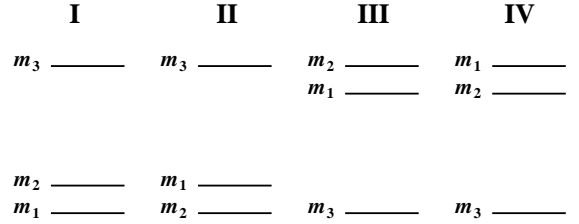


Figure 1. Schematic view of the four-types of neutrino-mass hierarchy.

is equivalent to the choice $0 \leq \theta_{12} \leq \pi/4$ and $0 \leq \theta_{13}, \theta_{23} \leq \pi/2$. In our convention ν_1 is defined by the condition $U_{e1} > U_{e2}$, and hence both $m_1 < m_2$ and $m_1 > m_2$ are allowed, and they should be determined by experiments.*Four possible patterns of the neutrino mass hierarchy are then defined as [11]

$$\begin{aligned} & (\delta m_{12}^2, \delta m_{13}^2) \quad (9) \\ & = (\delta m_{\text{SOL}}^2, \delta m_{\text{ATM}}^2) \quad (\text{I: normal hierarchy}) \\ & = (-\delta m_{\text{SOL}}^2, \delta m_{\text{ATM}}^2) \quad (\text{II}) \\ & = (\delta m_{\text{SOL}}^2, -\delta m_{\text{ATM}}^2) \quad (\text{III: inverted hierarchy}) \\ & = (-\delta m_{\text{SOL}}^2, -\delta m_{\text{ATM}}^2) \quad (\text{IV}) \end{aligned}$$

where $\delta m_{ij}^2 = m_j^2 - m_i^2$. See Fig. 1. The solar neutrino experiments determine

$$m_{12}^2 \equiv m_2^2 - m_1^2 = \delta m_{\text{SOL}}^2 > 0, \quad (10)$$

and hence only the hierarchy patterns I (normal) or III (inverted) are yet to be determined by future experiments.

We keep the four hierarchy cases in the following discussions because we find the following theorem [11,12] useful:

$$P_{\bar{\nu}_\alpha \rightarrow \bar{\nu}_\beta}^I = P_{\nu_\alpha \rightarrow \nu_\beta}^{IV} \quad (\text{normal hierarchy}), \quad (11a)$$

$$P_{\bar{\nu}_\alpha \rightarrow \bar{\nu}_\beta}^{III} = P_{\nu_\alpha \rightarrow \nu_\beta}^{II} \quad (\text{inverted hierarchy}) \quad (11b)$$

*This is equivalent to an alternative definition of ν_1 where $m_1 < m_2$ is assumed and the ordering $U_{e1} > U_{e2}$ or $U_{e1} < U_{e2}$ is to be determined by experiments.

The theorem is valid in the presence of an arbitrary matter profile [12]. Because of the theorem (11), we do not give expressions for the anti-neutrino oscillation probabilities explicitly. For instance, $P_{\bar{\nu}_\mu \rightarrow \bar{\nu}_e}$ in the normal hierarchy is obtained from the expression for $P_{\nu_\mu \rightarrow \nu_e}$ simply by reversing the sign of the factors Δ_{12} and Δ_{13} .

The probability of finding the flavor-eigenstate β from the original flavor-eigenstate α at the baseline length L in the vacuum is given by

$$\begin{aligned} & P_{\nu_\alpha \rightarrow \nu_\beta} \quad (12) \\ &= \left| \sum_{j=1}^3 (V_{\text{MNS}})_{\beta j} \exp \left(-i \frac{m_j^2}{2E_\nu} L \right) (V_{\text{MNS}})_{j\alpha} \right|^2 \\ &= |U_{\beta 1} U_{\alpha 1}^* + U_{\beta 2} e^{-i\Delta_{12}} U_{\alpha 2}^* + U_{\beta 3} e^{-i\Delta_{13}} U_{\alpha 3}^*|^2, \end{aligned}$$

where Δ_{ij} is

$$\Delta_{ij} \equiv \frac{\delta m_{ij}^2}{2E_\nu} L \simeq 2.534 \frac{\delta m_{ij}^2 (\text{eV}^2)}{E_\nu (\text{GeV})} L (\text{km}). \quad (13)$$

It is clear from this expression that the neutrino oscillation experiments cannot measure the two Majorana phases α_1 and α_2 in eq. (5), and that only the two mass squared differences out of the three neutrino masses can be probed by those experiments.

It is useful to give expressions of the oscillation probabilities when either Δ_{13} or Δ_{12} is order unity. For instance when $|\Delta_{13}| \sim O(1)$, we can expand the expressions in terms of $|\Delta_{12}| \ll 1$ and find

$$\begin{aligned} P_{\nu_\mu \rightarrow \nu_\mu} &= 1 - 4|U_{\mu 3}|^2(1 - |U_{\mu 3}|^2) \sin^2 \frac{\Delta_{13}}{2} \\ &+ 2|U_{\mu 2}|^2|U_{\mu 3}|^2 \sin \Delta_{13} \cdot \Delta_{12} + O((\Delta_{12})^2), \quad (14a) \end{aligned}$$

$$\begin{aligned} P_{\nu_e \rightarrow \nu_e} &= 1 - 4|U_{e 3}|^2(1 - |U_{e 3}|^2) \sin^2 \frac{\Delta_{13}}{2} \\ &+ 2|U_{e 2}|^2|U_{e 3}|^2 \sin \Delta_{13} \cdot \Delta_{12} + O((\Delta_{12})^2), \quad (14b) \end{aligned}$$

$$\begin{aligned} P_{\nu_\mu \rightarrow \nu_e} &= 4|U_{\mu 3}|^2|U_{e 3}|^2 \sin^2 \frac{\Delta_{13}}{2} \\ &+ 2\text{Re}[U_{\mu 2} U_{e 2}^* U_{e 3} U_{\mu 3}^*] \sin \Delta_{13} \cdot \Delta_{12} \\ &+ 4J_{\text{MNS}} \sin^2 \frac{\Delta_{13}}{2} \cdot \Delta_{12} + O((\Delta_{12})^2). \quad (14c) \end{aligned}$$

The expression eq. (14a) is relevant for the atmospheric neutrino oscillation and the K2K experi-

ment, and we may identify

$$\sin^2 2\theta_{\text{ATM}} = 4|U_{\mu 3}|^2(1 - |U_{\mu 3}|^2), \quad (15a)$$

$$\delta m_{\text{ATM}}^2 = |\delta m_{13}^2| = |m_3^2 - m_1^2|. \quad (15b)$$

The expression eq. (14b) is relevant for the reactor anti-neutrino oscillation experiments after the replacements in eq. (11) is made:

$$\sin^2 2\theta_{\text{RCT}} = 4|U_{e 3}|^2(1 - |U_{e 3}|^2), \quad (16a)$$

$$\delta m_{\text{RCT}}^2 = |\delta m_{13}^2| = \delta m_{\text{ATM}}^2. \quad (16b)$$

Only the magnitude of δm_{13}^2 is constrained because, so far no effects of order Δ_{12} have been positively identified. Finally, eq. (14c) is relevant for the $\nu_\mu \rightarrow \nu_e$ appearance experiments such as T2K. It is important to note that the $\nu_\mu \rightarrow \nu_e$ oscillation probability is proportional to

$$4 \sin^2 \theta_{\text{ATM}} \sin^2 \theta_{\text{RCT}} = 4|U_{\mu 3}|^2|U_{e 3}|^2. \quad (17)$$

and that the CP violating effect appears in the Δ_{12} order. The Jarlskog parameter of the MNS matrix is defined as

$$J_{\text{MNS}} \equiv \text{Im} (U_{\alpha i} U_{\beta i}^* U_{\beta j} U_{\alpha j}^*) \quad (18a)$$

$$= -\frac{U_{e 1} U_{e 2} U_{\mu 3} U_{\tau 3}}{1 - |U_{e 3}|^2} \text{Im} (U_{e 3}) \quad (18b)$$

$$= c_{13}^2 c_{12} c_{23} s_{12} s_{23} s_{13} \sin \delta_{\text{MNS}} \quad (18c)$$

where the orderings $(\alpha, \beta) = (e, \mu), (\mu, \tau), (\tau, e)$ and $(i, j) = (1, 2), (2, 3), (3, 1)$ should be taken in the definition. The expression (18b) follows from the convention (8) [10], and eq. (18c) follows from the parameterization (6) [5].

Comparison of the expansions in eq. (12) and the theorem (11) tells that the anti-neutrino oscillation probabilities have the same expressions as those for neutrinos up to terms of order Δ_{12} , except for the term proportional to J_{MNS} . We find

$$\begin{aligned} & P_{\nu_\mu \rightarrow \nu_e} - P_{\bar{\nu}_\mu \rightarrow \bar{\nu}_e} \\ &= 8J_{\text{MNS}} \sin^2 \frac{\Delta_{13}}{2} \cdot \Delta_{12} + O((\Delta_{12})^2), \quad (19) \end{aligned}$$

which is valid for both normal and inverted hierarchies. Although the above expression is valid only when we can neglect the earth matter effects

of the oscillation probabilities, it gives a good zeroth order approximation to the proposed T2K and T-to-HK experiments, which plan to use sub-GeV neutrino beams.

When the magnitude of Δ_{12} is of the order of unity, $|\Delta_{13}| \sim \delta m_{\text{ATM}}^2 / \delta m_{\text{SOL}}^2 \sim 30 \gg 1$ applies, and we have an alternative expansion of eq. (12). The most relevant one is

$$P_{\nu_e \rightarrow \nu_e} = 1 - 4|U_{e1}|^2|U_{e2}|^2 \sin^2 \frac{\Delta_{12}}{2} - \frac{1}{2} \sin^2 2\theta_{\text{RCT}} + O\left(\frac{E_\nu}{\delta E_\nu \Delta_{13}}\right), \quad (20)$$

where $\delta E_\nu / E_\nu$ is the experimental resolution of the neutrino energy. The expression (20) is relevant for the solar neutrino oscillation and the KamLand reactor neutrino oscillation experiments. By neglecting the small term proportional to $\sin^2 2\theta_{\text{RCT}}$, we can identify

$$\sin^2 2\theta_{\text{SOL}} = 4|U_{e2}|^2|U_{e1}|^2, \quad (21a)$$

$$\delta m_{\text{SOL}}^2 = |\delta m_{12}^2| = |m_2^2 - m_1^2|. \quad (21b)$$

The sign of the mass squared difference cannot be determined from the above expression, which applies for the KamLand experiments.

From the above arguments, we can parameterize the complete MNS matrix elements by using the observed constraints on the three mixing angles:

$$|U_{e3}|^2 = \frac{1 - \sqrt{1 - \sin^2 2\theta_{\text{RCT}}}}{2},$$

$$U_{e2}^2 = \frac{1 - |U_{e3}|^2 - \sqrt{(1 - |U_{e3}|^2)^2 - \sin^2 2\theta_{\text{SOL}}}}{2},$$

$$U_{\mu 3}^2 = \frac{1 \pm \sqrt{1 - \sin^2 2\theta_{\text{ATM}}}}{2}. \quad (22)$$

Since the magnitudes of the three matrix elements at the corner of the MNS matrix are determined as above, the full MNS matrix can be determined for a given CP phase δ_{MNS} [10]. Although the above identifications are valid only approximately, they suffice for our discussions about physics prospects of future neutrino oscillation experiments.

2. Matter effects in the neutrino oscillation

The neutrino mass hierarchy pattern between I and II (III and IV) has been distinguished by the matter effects of the observed solar neutrino oscillation.

The oscillation probabilities in the matter has the same form as in eqs. (12), (13) and (14), where the mass-squared differences and the MNS matrix elements are replaced by those in the matter:

$$\Delta_{ij} \rightarrow \tilde{\Delta}_{ij}, \quad U_{\alpha i} \rightarrow \tilde{U}_{\alpha i}, \quad J_{\text{MNS}} \rightarrow \tilde{J}_{\text{MNS}}, \quad (23)$$

if the variation of the matter density remains small along the base-line.

Neutrino-flavor oscillation inside of the matter is governed by the equation [13,14]

$$i \frac{\partial}{\partial t} \begin{pmatrix} \nu_e \\ \nu_\mu \\ \nu_\tau \end{pmatrix} = \frac{1}{2E_\nu} H \begin{pmatrix} \nu_e \\ \nu_\mu \\ \nu_\tau \end{pmatrix}, \quad (24a)$$

where the Hamiltonian (in units of $2E_\nu$) in the matter is

$$H = U \text{ diag}(0, \delta m_{12}^2, \delta m_{13}^2) U^\dagger + \text{diag}(a, 0, 0) \quad (24b)$$

$$= \tilde{U} \begin{pmatrix} \lambda_1 & 0 & 0 \\ 0 & \lambda_2 & 0 \\ 0 & 0 & \lambda_3 \end{pmatrix} \tilde{U}^\dagger. \quad (24c)$$

Here a is the matter effect term,

$$a = 2\sqrt{2}G_F n_e E_\nu$$

$$= 7.56 \times 10^{-5}(\text{eV}^2) \left(\frac{\rho}{\text{g/cm}^3} \right) \left(\frac{E_\nu}{\text{GeV}} \right), \quad (25)$$

where n_e is the electron density, G_F is the Fermi constant, and ρ is the matter density.

The Hamiltonian H in the matter is diagonalized by the MNS matrix in the matter \tilde{U} . The neutrino-flavor oscillation probabilities in the matter take the same form as those in the vacuum by making the replacement (23) where

$$\tilde{\Delta}_{ij} = \frac{\lambda_j - \lambda_i}{2E_\nu} L \equiv \frac{\delta \tilde{m}_{ij}^2}{2E_\nu} L. \quad (26)$$

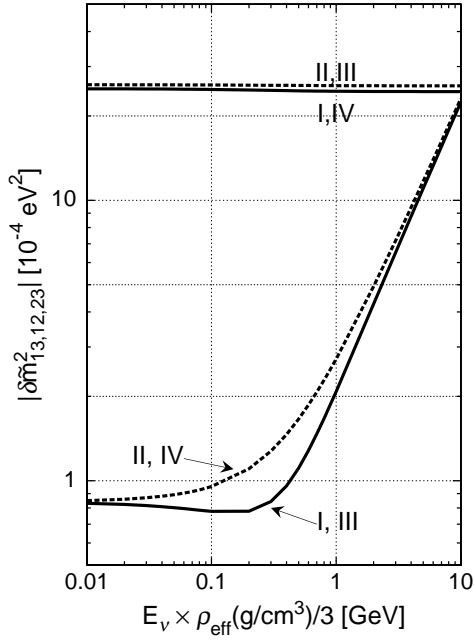


Figure 2. The magnitudes of the effective mass squared differences, $|\delta\tilde{m}_{13}^2|$ ($|\delta\tilde{m}_{23}^2|$ in the hierarchy II, IV cases) and $|\delta\tilde{m}_{12}^2|$, as functions of the neutrino energy times the effective matter density $\rho_{\text{eff}}(\text{g}/\text{cm}^3)/3$. In the earth crust, $\rho_{\text{eff}} \sim 3$, and at the center of the sun, $\rho_{\text{eff}} \sim 200$.

In Fig. 2, we show the E_ν -dependence of the magnitudes of the effective mass-squared differences, $|\delta\tilde{m}_{13}^2|$ and $|\delta\tilde{m}_{12}^2|$ for the 4 mass hierarchy cases of Fig. 1. In case of the hierarchy II and IV, we show $|\delta\tilde{m}_{23}^2|$ rather than $|\delta\tilde{m}_{13}^2|$, because the leading oscillation term is dictated by the former difference. The curves are obtained for

$$|\delta m_{13}^2| = 2.5 \times 10^{-3} \text{ eV}^2, \quad (27a)$$

$$|\delta m_{12}^2| = 8.3 \times 10^{-5} \text{ eV}^2, \quad (27b)$$

$$\tan^2 \theta_{\text{SOL}} = 0.4, \quad (27c)$$

$$\sin^2 \theta_{\text{RCT}} = 0. \quad (27d)$$

It is worth noting that the matter effects depend only on the above four parameters, i.e., the two mass squared differences and the two angles, θ_{12}

and θ_{13} , because of the identity [15]

$$H = O_{23} P_\delta H' P_\delta^\dagger O_{23}^T, \quad (28a)$$

where

$$H' = O_{13} O_{12} \text{diag}(0, \delta m_{12}^2, \delta m_{13}^2) O_{12}^T O_{13}^T + \text{diag}(a, 0, 0). \quad (28b)$$

It is clear that the above reduced Hamiltonian H' can be diagonalized as

$$H' = \tilde{O} \text{diag}(\lambda_1, \lambda_2, \lambda_3) \tilde{O}^T, \quad (29a)$$

with the same eigen values of H in eq. (24b). The MNS matrix in the matter is then expressed as[†]

$$\tilde{U} = O_{23} P_\delta \tilde{O}. \quad (29b)$$

In the limit of $\sin^2 \theta_{\text{RCT}} = (s_{13})^2 = 0$ in eq. (27), the matrix $O_{13} = 1$, and the eigen value problem is reduced to the 2×2 matrix problem. The eigenvalues are

$$\lambda_\pm = \frac{\delta m_{12}^2 + a \pm \sqrt{(\delta m_{12}^2 + a)^2 - 4a c_{12}^2 \delta m_{12}^2}}{2},$$

$$\lambda_3 = \delta m_{13}^2, \quad (30)$$

and the results are shown in Fig. 2 for all the four hierarchy cases of Fig. 1. Note that

$$(\lambda_1, \lambda_2) = (\lambda_-, \lambda_+) \text{ hierarchy I, III}, \quad (31a)$$

$$= (\lambda_+, \lambda_-) \text{ hierarchy II, VI}, \quad (31b)$$

so that $\lambda_1 \rightarrow 0$ and $\lambda_2 - \lambda_1 = \delta\tilde{m}_{12}^2 \rightarrow \delta m_{12}^2$ in the $a \rightarrow 0$ limit. Although all the curves in Fig. 2 are obtained in the limit of $\sin^2 \theta_{\text{RCT}} = 0$, we find that the qualitative features of the curves remain the same even when $\sin^2 2\theta_{\text{RCT}} \approx 0.1$, except near the 10 GeV region.

The horizontal scale of Fig. 2 is the neutrino energy times the effective matter density in units of $3 \text{ g}/(\text{cm}^3)$, and the vertical scale gives the magnitudes of the effective mass squared differences in the matter. The typical energy of the reactor anti-neutrinos is about a few MeV, or a few

[†]Note that once the expression (29b) is used to calculate the MNS matrix in the matter, the phase convention of eq. (8) is no more valid.

$\times 10^{-3}$ GeV, and hence there is no significant difference between the hierarchy I and II (or between III and IV) in the CHOOZ or KamLand experiments. On the other hand, the typical Boron (^8B) neutrino flux energy of 7 MeV with the effective matter density of $\rho_{\text{eff}} < 200 \text{ g}/(\text{cm})^3$ in the sun extends up to 450 MeV in the horizontal scale, where the matter effects clearly distinguish between the neutrino mass hierarchies, and the energy dependence of the observed solar neutrino flux clearly favors the hierarchy I or III, over II or IV. In fact, in case of the hierarchy I or III, the effective mass squared difference

$$\begin{aligned} |\delta\tilde{m}_{12}^2| &= |\lambda_2 - \lambda_1| \\ &= \sqrt{(a - \cos 2\theta_{12} \delta m_{12}^2)^2 + (\cos 2\theta_{12} \delta m_{12}^2)^2} \end{aligned} \quad (32)$$

has the minimum at

$$a = \cos 2\theta_{12} \delta m_{12}^2 \quad (33)$$

where the effective mixing angle $\tilde{\theta}_{12}$ crosses $\pi/4$. On the other hand, in case of the hierarchy II or IV, since $\delta m_{12}^2 < 0$ in eq. (32), there is no minimum, and the effective mixing angle decreases at high energy or density. The difference is significant enough to affect the observed energy spectrum of the solar neutrino flux on the earth, and the neutrino mass hierarchy I or III has been chosen against II or IV.

Between the hierarchy I (normal) and III (inverted), the difference in the matter effects remains small for the effective mass squared differences in Fig. 2. The ongoing K2K experiment with the baseline length of 250 km and the planned long baseline neutrino oscillation experiments T2K, from J-PARC at Tokai to Kamioka, whose baseline length is about 300 km, adopt rather low energy neutrino beam below 1 GeV, where the matter effect is rather small. We will find below that the remaining ambiguity between the neutrino mass hierarchy I (normal) and III (inverted) can be distinguished by using the earth matter effects at higher energy very long baseline neutrino oscillation experiments.

3. T2K and T-to-HK projects

The proposed long-baseline (LBL) neutrino-oscillation experiments [16,17] will achieve the precision measurements of δm_{ATM}^2 and $\sin^2 2\theta_{\text{ATM}}$ by using conventional neutrino beams, which are made from decays of π and K that are produced by high-energy proton beams. In particular, the T2K experiment will be able to detect $\nu_\mu \rightarrow \nu_e$ appearance, if the magnitude of the oscillation eq. (17) is not too small.

The T2K neutrino beam line is now under construction at J-PARC (Japan Proton Accelerator Research Complex) in Tokai village [18], whose 50 GeV high intensity proton accelerator with 0.75 MW will deliver 10^{21} POT (proton on target) per year. This is about a factor of 50 more intensive than the KEK proton synchrotron for the present K2K experiment. Since Tokai village is about 50 km east from KEK, the baseline length of the T2K experiment will be $L = 295$ km, as compared to $L = 250$ km for K2K: see Fig. 3. They plan to make use of the K2K proven technique to reconstruct neutrino energy at Super-Kamiokande (SK) by selecting quasi-elastic charged current events. The expected accuracy is

$$\Delta(|\delta m_{13}^2|) = 10^{-4} \text{ eV}^2, \quad (34a)$$

$$\Delta(\sin^2 2\theta_{\text{ATM}}) = 0.01, \quad (34b)$$

from the precision measurement of the deficit of the ν_μ flux. Because SK is capable of detecting ν_e charged current events clearly, they will have a good sensitivity to the $\nu_\mu \rightarrow \nu_e$ appearance measurement if

$$\sin^2 2\theta_{\text{RCT}} \gtrsim 0.006. \quad (35)$$

Even with the intensive proton beam from J-PARC, it is not an easy task to measure the oscillation probabilities for anti-neutrinos because the charged current cross section of anti-neutrinos is a factor of 3 smaller than the neutrino cross sections. A factor of 5 upgrade in the power of the proton beam to 4MW, and a factor of 50 larger detector, 1 Mton water Čerenkov detector Hyper-Kamiokande (HK) are therefore envisaged [19].

In Ref.[20], we studied the possibility of measuring δ_{MNS} in the future T-to-HK experiment.



Figure 3. The long baseline neutrino oscillation projects, K2K (KEK to Super-Kamiokande; 250km) and T2K (J-PARC at Tokai to Super-Kamiokande; 295km).

There the measurement of the difference (19) by making use of both the neutrino (ν_μ enriched) beam and the anti-neutrino ($\bar{\nu}_\mu$ enriched) beam allows us to study CP violation in the lepton sector. We find that the advantage of the T-to-HK experiment over various proposed neutrino oscillation experiments lies in the fact that the water Čerenkov detector is capable of measuring both μ and e charged current reactions, and that the use of low energy beam (of order 1 GeV or less) at relatively short distances (295 km) makes the matter effects small. Because of the above advantages, the experiment can effectively measure the difference (19), and hence have high sensitivity to the CP violating leptonic Jarlskog parameter J_{MNS} of eq. (18), or $\sin \delta_{\text{MNS}}$. For instance, it is relatively easy to distinguish between $\delta_{\text{MNS}} = 90^\circ$ and $\delta_{\text{MNS}} = 270^\circ$. On the other hand, we found that it is a non-trivial task for the experiment to distinguish between

$$\delta_{\text{MNS}} \text{ vs } \pi - \delta_{\text{MNS}}, \quad (36)$$

most notably, between $\delta_{\text{MNS}} = 0^\circ$ and $\delta_{\text{MNS}} = 180^\circ$. In order to distinguish between the two cases in eq. (36), which give the same $\sin \delta_{\text{MNS}}$, we

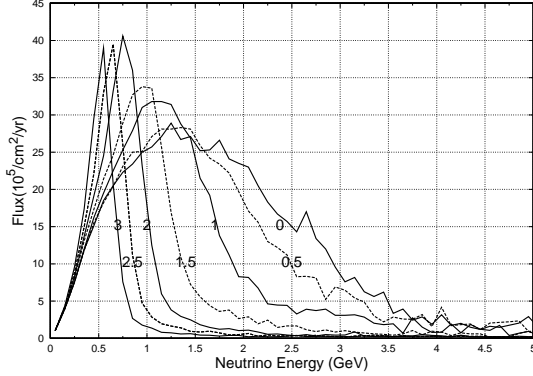


Figure 4. The neutrino beam flux from J-PARC at $L=295\text{km}$ for different off-axis angles, 3, 2.5, 2, 1.5, 1, 0.5 and 0 degree (on axis).

should measure $\cos \delta_{\text{MNS}}$ as well. In the $\nu_\mu \rightarrow \nu_e$ transition probability expression of eq. (14c), the relevant term is

$$2Re[U_{\mu 2}U_{e 2}^*U_{e 3}U_{\mu 3}^*] \sin \Delta_{13} \cdot \Delta_{12}, \quad (37)$$

whose magnitude is small at around $\Delta_{13} \sim \pi$ where the leading $\sin^2(\Delta_{13}/2)$ term takes its maximum value of unity. In order to distinguish this sub-leading term from the leading one, we need to make experiments at different neutrino energies. By choosing the neutrino narrow band beam at two different energies, we could show in ref. [20] that the degeneracy between $\delta_{\text{MNS}} = 0^\circ$ and 180° can be resolved.

After our work [20] was completed in 2002, the T2K collaboration decided to adopt the off-axis beam (OAB) rather than the narrow band beam (NBB) which was used in our analysis. The OAB flux has a sharp peak at low energies and has relatively long high-energy tail. The flux intensity of the OAB around the sharp peak is typically stronger than that of the NBB, while the hard high energy tail may be considered as a disadvantage. We show the OAB flux profile from the J-PARC 50 GeV proton accelerator in Fig. 4. Fluxes at off-axis angles between 0° (on-axis) and 3° are shown for later use. For the T2K and T-to-HK experiments, the neutrino beam line at J-

PARC has been set up such that the OAB beam between 2° and 3° can be sent to SK and HK. The beam orientation has been so chosen that once HK is constructed at its planned location, exactly the same OAB will hit both detectors. We may read off from the figure that the peak flux energy is about 0.8, 0.7, and 0.6 GeV for 2° , 2.5° , and 3° , respectively. The larger the OAB angle, the lower the peak energy is, and sharper the cut-off for the high-energy tail.

By repeating the analysis of ref. [20] for the experimental setup of

$$0.8 \text{ Mton} \cdot \text{year for } \nu_\mu \text{OAB}(2^\circ), \quad (38a)$$

$$2.0 \text{ Mton} \cdot \text{year for } \nu_\mu \text{OAB}(3^\circ), \quad (38b)$$

$$3.2 \text{ Mton} \cdot \text{year for } \bar{\nu}_\mu \text{OAB}(2^\circ), \quad (38c)$$

we find the results of Fig. 5. The flux ratios are so chosen that roughly the same number of charged current events are expected, about 10^4 μ -like events and about a few hundreds to a thousand e -like events, in the range of the parameter space we studied. If a factor of 5 more intensive beam is available at J-PARC by the time we will have HK, the same quality results may be obtained in less than one and a half year time.

The contours of Fig. 5 show the 1-, 2-, and 3- σ allowed region in the plane of $\sin^2 2\theta_{\text{RCT}}$ and δ_{MNS} . They are obtained as follows. We first calculate the expected numbers of μ -like and e -like events at HK for the following input parameter values:

$$\delta m_{\text{ATM}}^2 = 3 \times 10^{-3} \text{ eV}^2, \quad (39a)$$

$$\delta m_{\text{SOL}}^2 = 7 \times 10^{-5} \text{ eV}^2, \quad (39b)$$

$$\sin^2 2\theta_{\text{ATM}} = 1, \quad (39c)$$

$$\sin^2 2\theta_{\text{SOL}} = 0.85, \quad (39d)$$

$$\sin^2 2\theta_{\text{RCT}} = 0.01 \text{ or } 0.06, \quad (39e)$$

$$\delta_{\text{MNS}} = 0^\circ, 90^\circ, 180^\circ \text{ or } 270^\circ, \quad (39f)$$

by assuming the constant matter density of $\rho = 3\text{g}/(\text{cm}^3)$ along the baseline. The resulting number of events are then analyzed by varying all the 6 parameters under the known constraints for the four parameters δm_{ATM}^2 , $\sin^2 2\theta_{\text{ATM}}$, δm_{SOL}^2 , and $\sin^2 2\theta_{\text{SOL}} = 4 \tan^2 \theta_{\text{SOL}} / (1 + \tan^2 \theta_{\text{SOL}})^2$, and by allowing for 3% normalization uncertainties in the earth matter density and the overall beam flux.

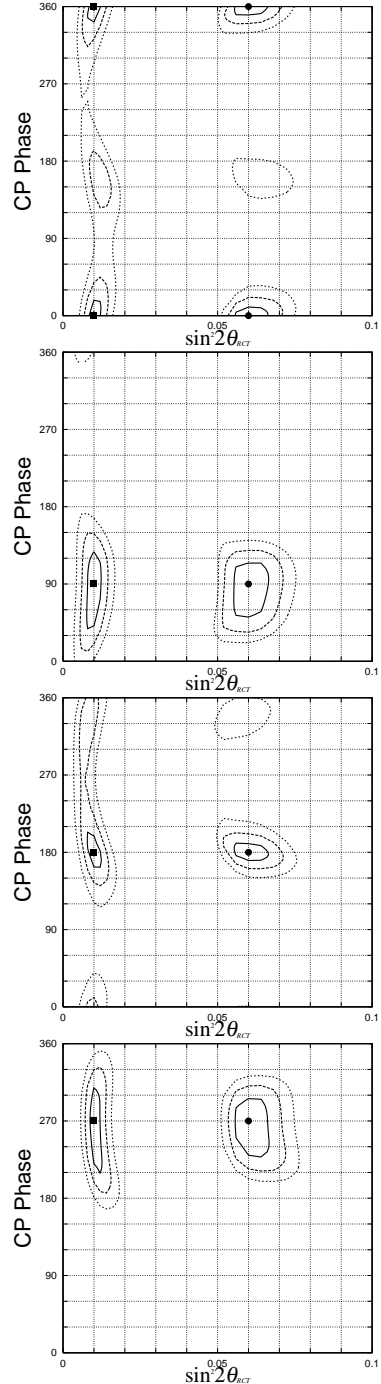


Figure 5. Allowed regions in the plane of $\sin^2 2\theta_{\text{RCT}}$ and δ_{MNS} after 6 years of T-to-HK.

In addition, some of the known systematic errors from the SK and K2K experiences were taken into account.

We find from Fig. 5 that the T-to-HK experiment can establish CP violation at the 3σ level if $\delta_{\text{MNS}} \sim 90^\circ$ or 270° . Also, the use of both 2° and 3° OAB can contribute to resolving the degeneracy between $\delta_{\text{MNS}} \sim 0^\circ$ or 180° if $\sin^2 2\theta_{\text{RCT}}$ is not too small. When comparing the contours of Fig. 5 with the corresponding results of ref. [20] which were obtained for the narrow-band beams (NBB), however, we find that the areas of the 3σ allowed regions are significantly wider for the OAB than the NBB and that the capability of distinguishing between the 0° and 180° degeneracy is lower for the OAB. These results are obtained even though the typical flux of OAB is higher than that of NBB, mainly because of much higher background of the OAB, especially in the high energy tail. The background is found most serious for the $\bar{\nu}_\mu \rightarrow \bar{\nu}_e$ measurements where the ν_e component of the $\bar{\nu}_\mu$ enriched beam contributes to the e -like signal since HK cannot distinguish the charge. We find that the background level is significant in the high energy tail of the OAB, and hence rejection of events with high neutrino energies can improve the measurement. Our studies on the T-to-HK experiments with OAB will be reported in [21] soon.

4. The parameter degeneracy problem

Those studies, however, assumed that the neutrino mass hierarchy is known to be normal ($\delta m_{13}^2 = \delta m_{\text{ATM}}^2$) and also we assumed $\sin^2 \theta_{\text{ATM}} = 0.5$ as an input.

In particular, our results for $\delta_{\text{MNS}} = 90^\circ$ and 270° in Fig. 5 suggest that the T-to-HK experiment can establish CP violation at the 3σ level or higher, if $\sin^2 2\theta_{\text{RCT}}$ is not too small. We find, however, that this observation depends critically on the assumption that we know the neutrino mass hierarchy to be normal, i.e., the hierarchy pattern I in Fig. 1.

As a demonstration, we show in Fig. 6(a) the allowed region of the T-to-HK simulation by analyzing exactly the same input ‘data’, calculated for the normal hierarchy ($\delta m_{13}^2 > 0$), by assum-

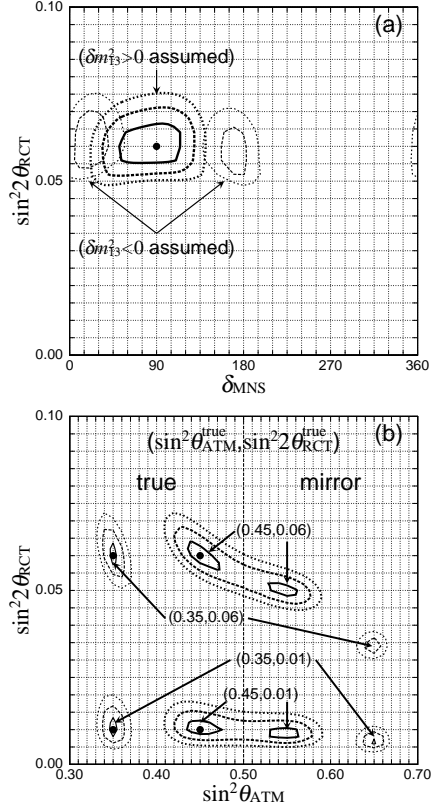


Figure 6. Doubling of the regions allowed by future LBL experiment T-to-HK, between J-PARC at Tokai and HyperKamiokande, in the plane of δ_{MNS} and $\sin^2 2\theta_{\text{RCT}}$ (a), and $\sin^2 \theta_{\text{ATM}}$ and $\sin^2 2\theta_{\text{RCT}}$ (b).

ing that the neutrino mass hierarchy is inverted ($\delta m_{13}^2 < 0$). We find the region encircled by thin lines from this analysis. The minimum of the χ^2 value in those regions are only slightly larger than unity, and hence the solutions cannot be excluded by the measurements. Most strikingly, the allowed regions obtained by assuming the inverted hierarchy give $\delta_{\text{MNS}} \sim 0^\circ$ or 180° , i.e., the very conclusion of the evidence of CP violation in the lepton sector depends on our capability of distinguishing between the two remaining hierarchy cases, I (normal) or III (inverted).

There is one more hidden degeneracy problem among the 6 parameters of the 3 neutrino model. It is the magnitude of $\sin^2 \theta_{\text{ATM}} = |U_{\mu 3}|^2$ which has a two-fold ambiguity

$$\sin^2 \theta_{\text{ATM}} = |U_{\mu 3}|^2 = \frac{1 \pm \sqrt{1 - \sin^2 2\theta_{\text{ATM}}}}{2} \quad (40)$$

in the last line of eq. (22). The two-fold ambiguity was hidden so far because we chose the extreme value of $\sin^2 2\theta_{\text{ATM}} = 1$ as our input. It should be remarked that the presently allowed range of $\sin^2 2\theta_{\text{ATM}} > 0.90$ in eq. (1) corresponds to

$$0.34 < \sin^2 \theta_{\text{ATM}} < 0.65. \quad (41)$$

In Fig. 6(b), we showed the allowed region in the same T-to-HK simulation, when the input data are calculated for

$$\sin^2 \theta_{\text{ATM}} = 0.35 \text{ or } 0.45 \quad (42)$$

instead of $\sin^2 \theta_{\text{ATM}} = 0.5$ in eq. (39). In addition to the correct solutions which are marked by the solid blob at the input points, we find a mirror solution at the $\sin^2 \theta_{\text{ATM}}$ value corresponding to the opposite sign in eq. (40) for the same $\sin^2 2\theta_{\text{ATM}}$ value. We notice also that the mirror solutions appear at different values of $\sin^2 2\theta_{\text{RCT}}$, and hence the measurement of $\sin^2 2\theta_{\text{RCT}}$ at T2K and in the future T-to-HK experiments also suffer from this degeneracy problem. The reason for the correlation between $\sin^2 \theta_{\text{ATM}}$ and $\sin^2 2\theta_{\text{RCT}}$ is a manifestation of the fact that the magnitude of the leading term that dictates the $\nu_\mu \rightarrow \nu_e$ oscillation probability (14c) is their product in eq. (17). This correlation suggests that if we can measure $\sin^2 2\theta_{\text{RCT}}$ that governs the leading term of the $\nu_e \rightarrow \nu_e$ oscillation in eq. (14b) accurately independent of the magnitude of $\sin^2 \theta_{\text{ATM}}$, we can resolve the ambiguity.

These studies demonstrate clearly that we need more works to do in order to determine the neutrino mass hierarchy pattern between the normal (I) and inverted (III) ones, and to determine the third mixing angle $\sin^2 2\theta_{\text{RCT}}$ and $\sin^2 \theta_{\text{ATM}}$ independently. New generations of the reactor neutrino experiments, such as Double-CHOOZ [22] and KASKA [23] have been proposed to tackle the

latter problem. In the rest of this talk, I would like to introduce our studies about possible future long baseline neutrino oscillation experiments in Asia, which make use of neutrino beams from the J-PARC facility.

5. Fate of the T2K and T-to-HK beam

We first study the fate of the off axis beam of the T2K and the possible T-to-HK project. The OAB at J-PARC is shoot underground, such that exactly the same OAB will be available at the present SK site and the planned HK site. The center of the beam at around Kamioka site passes through more than 10 km deep in the earth crust. The beam center will re-appear on the earth surface in the middle of the Japan sea, and the OAB of the off-axis angle between 0.5° and 3° will be available free in Korea. The surface view of the OAB(2.5°) is shown in Fig. 8 and the vertical cross section view of the beam is shown in Fig. 9.

In the surface view of Fig. 8, the red curves show the contours of the same baseline length. The solid and dashed black contours give the off-axis angle. The center of the beam is at 0° , which appears in the Japan sea, a few hundred km east from the Korean coast. Inside of Korea mainland, the off-axis beam of 1° to 3° is available at $L = 1,000$ km to $1,200$ km. The off axis beam at 0.5° is available at the Korean east coast, for the OAB(3°) at Kamioka.

Therefore, depending on the location of a possible neutrino detector in Korea, the flux of off-axis angle between 0.5° and 3° shown in Fig. 4 will be available during the period of the T2K experiment, and possibly during the T-to-HK experiment. Because the flux at $L \sim 1,000$ km to $1,200$ km is about a factor of 10 to 16 smaller than that at Kamioka, respectively, we may need a detector of 100 kton volume in order to obtain significant new contributions.

Because the OAB at large angles has a sharp peak at low energies, see Fig. 4, one may study the oscillation probabilities at large L/E . There are a few advantages of neutrino oscillation experiments at large L/E while keeping the neutrino energy at sub-GeV.

- Δ_{12} grows with L/E , and hence the sensi-

tivity to δ_{MNS} in the $\nu_\mu \rightarrow \nu_e$ experiment will grow; see eq. (14c).

- The sign of the term linear in both Δ_{12} and Δ_{13} determines the neutrino mass hierarchy, because the term $\Delta_{12} \cdot \Delta_{13}$ is positive for the normal hierarchy (I), while it is negative for the inverted hierarchy (III).

Relative smallness of the earth matter effects at lower energies will be helpful in the study, since the above features of the $\nu_\mu \rightarrow \nu_e$ oscillation probability can be read off from the expansion in terms of Δ_{12} in eq. (14c) which is a good approximation only up to a few GeV; see Fig. 2.

In Fig. 7, we show the oscillation probabilities $P(\nu_\mu \rightarrow \nu_e)$ and $P(\bar{\nu}_\mu \rightarrow \bar{\nu}_e)$ for $E_\nu = 0.7$ GeV plotted against the baseline length L . The upper two figures are for the normal hierarchy (I) and the lower two are for the inverted hierarchy (III). We can see from the figure that in some cases, small differences at $L = 300$ km for the T2K and T-to-HK experiments can be enhanced significantly in Korea between $L = 1,000$ km and 1,200 km. The difference between the normal and inverted hierarchy can be very significant and there is a hope that a combination of the T-to-HK measurement and the T-to-Korea experiment can resolve the ambiguity in the δ_{MNS} and the neutrino mass hierarchy cases at the same time. The study is underway [24].

At the moment, we do not know if there is a strong interest in constructing a huge neutrino detector in Korea. Because we feel that this investigation is rather promising, we study the fate of the OAB from J-PARC in the T2K experiment carefully. Although only the fate of the OAB(2.5°) is shown in Fig. 8 and Fig. 9, we made similar figures for OAB(2°) and OAB(3°). In case of OAB(2°), the smallest off-axis angle at the east coast of Korea is about 1.5° , while for OAB(3°), the smallest angle is about 0.5° .

In the cross section view of Fig. 9, we show the baseline, along the direction of J-PARC at Tokai village to the center of the SK and the proposed HK site in Kamioka. The OAB(2.5°) beam hits SK and HK at the same off-axis angle of 2.5° , while the beam center (0°) reaches the earth surface in the sea. It is rather important to rec-

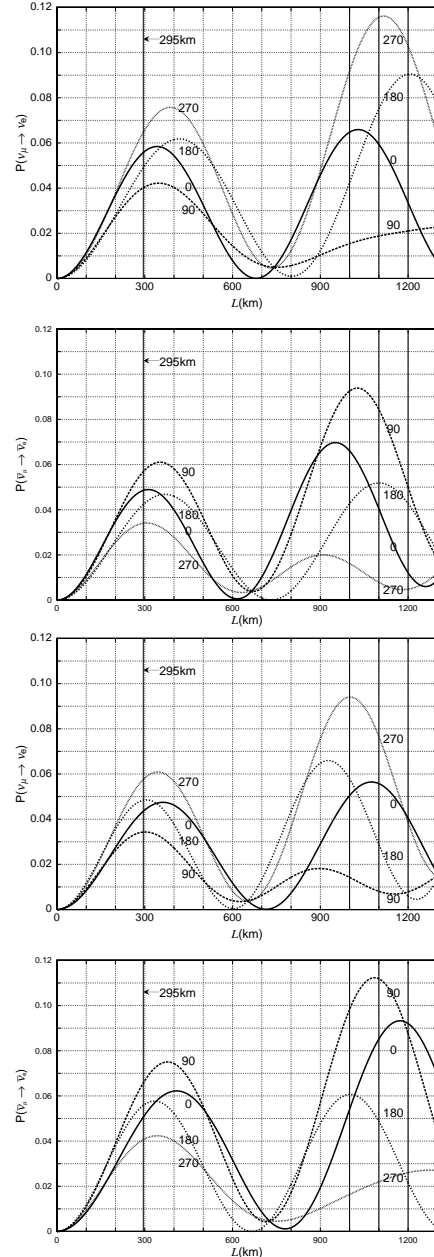


Figure 7. The oscillation probabilities $P(\nu_\mu \rightarrow \nu_e)$ and $P(\bar{\nu}_\mu \rightarrow \bar{\nu}_e)$ for $E_\nu = 0.7$ GeV plotted against the baseline length L . The upper two figures are for the normal hierarchy (I) and the lower two are for the inverted hierarchy (III).

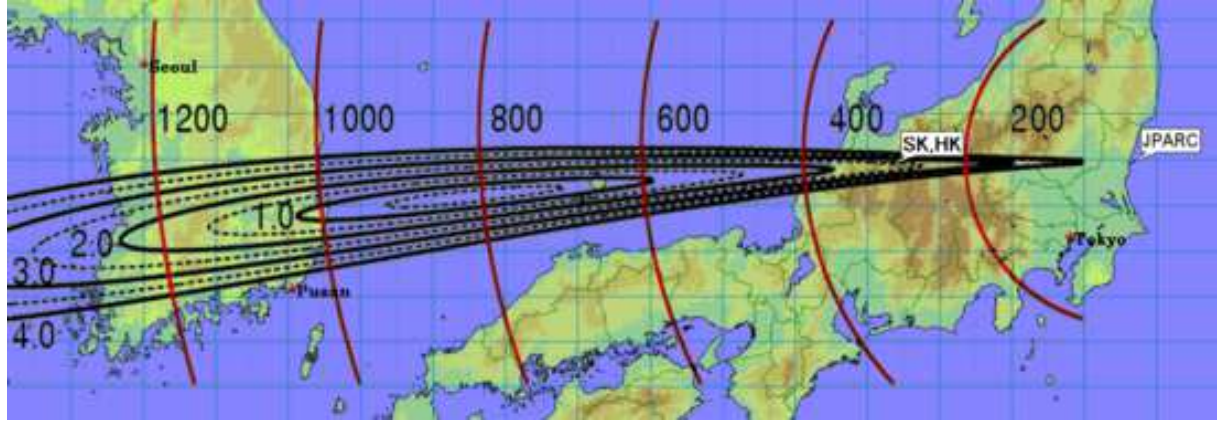


Figure 8. The fate of the OAB 2.5 degree beam from J-PARC. Surface view.

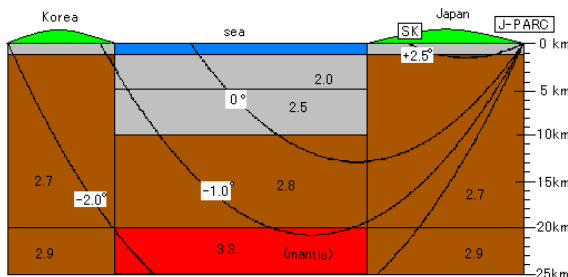


Figure 9. The fate of the OAB 2.5 degree beam from J-PARC. Vertical view.

ognize that the Japan sea is rather shallow, and the beams which reach Korea do not travel under water. The numerics in the earth crust show the effective mass density ρ in units of $\text{g}/(\text{cm})^3$. We can view that under the sea the earth crust is thin, and the mantle appears already at 20 km beneath the earth surface. The density variations, however, are not expected to be significant. We hope that our studies [24] will be found useful by our colleagues in Korea.

6. High energy super beam to China

Although we do not yet know if there are strong enough interests in constructing a huge neutrino detector in Korea, strong interests have been expressed by our Chinese colleagues about the possibility of sending super neutrino beams from J-PARC at Tokai to somewhere in mainland China. A possible 100 kton level water Čerenkov detector BAND (Beijing Astrophysics and Neutrino Detector) [25] has been proposed, and if it will be placed in Beijing, the baseline length from Tokai will be about $L=2,100$ km. The unique capability of the BAND detector is that it is a segmented detector, where each segment contains 10 ton of water surrounded by the photo-multiplier tube to measure the Čerenkov light, and at the same time has a good capability of calorimetric energy measurement [25].

Encouraged by the interests expressed by our Chinese colleagues, we made a serious study of physics capability of a very long baseline neutrino oscillation experiments between J-PARC at Tokai and BAND in Beijing [11]. The global view of the eastern Asia seen from J-PARC at Tokai is shown in Fig. 10. It is clearly seen from the figure that the LBL experiments with L greater than 2,000 km are feasible if a huge neutrino detector can be built in China. We can also tell



Figure 10. East Asia viewed from J-PARC in Tokai. The baseline length $L = 295$ km (Kamioka), 1,200 km (Seoul) and 2,100 km (Beijing).

from the figure that the direction from Tokai to Kamioka is almost exactly from east to west, and the T2K beam goes through southern part of Korea. Since Beijing is placed north east from the T2K beam-line, a new neutrino beam line toward Beijing should be constructed at J-PARC.

In addition, in order to send sufficient neutrino flux to the distance greater than 2,000 km, and in order to study physics at the same L/E region where the first oscillation mode takes its maximum value,

$$|\Delta_{13}| \sim \pi \text{ when } L(\text{km})/E(\text{GeV}) \sim 500, \quad (43)$$

for $\delta m_{\text{ATM}}^2 = 2.5 \times 10^{-3} \text{ eV}^2$, we need a neutrino beam whose flux peaks at around 3 to 6 GeV. Such neutrino beams can indeed be designed for the J-PARC 50 GeV proton accelerator, and has been named HENBB (High Energy Narrow Band Beam) in ref. [11]. We show in Fig. 11 the expected flux times the neutrino energy E_ν as functions of E_ν . We multiply the flux by E_ν in order to show the peak in the expected number of events in the absence of the neutrino oscillation. The peak position of the flux $\times E_\nu$ is called E_p

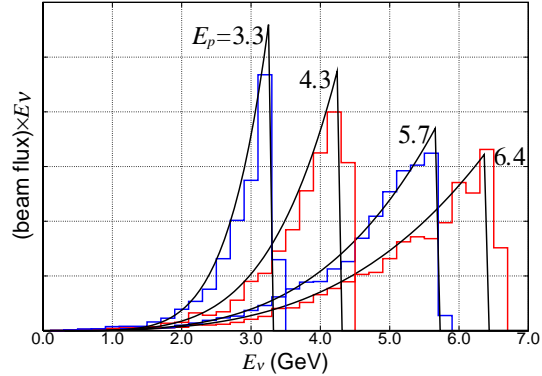


Figure 11. High energy narrow band beams (HENBB) at J-PARC for the possible T2B (Tokai-to-Beijing) project.

and the simulation results are shown for $E_p = 3.3, 4.3, 5.7$ and 6.4 GeV. The optics adopted for generating the HENBB makes the peak rather sharp, especially in the high energy side. This sharp cut-off of the high energy neutrinos makes the background level low when the HENBB is used for the LBL experiments. In fact we find that the largest background from the high energy neutrinos beyond E_p comes mainly from the contribution from the $K \rightarrow \mu\nu$ decays, which may be measured precisely at a near detector. We made a parameterization of the HENBB flux for a given E_p in order to save time for the beam simulation, and the parameterization is given in ref. [11].

We show in Fig. 12, the expected total numbers of the e -like events and the μ -like events. Since we do not require the charge identification capability for the BAND detector[‡] the μ -like events are the sum of ν_μ and $\bar{\nu}_\mu$ charged current (CC) events and the e -like events are the sum of ν_e and $\bar{\nu}_e$ CC events and those expected from the NC events where produced π^0 's are mistaken as e^\pm . At higher energies, τ production from the

[‡]Possibility of putting the segmented water Čerenkov detector of BAND under the magnetic field has been studied by the IHEP group [25].

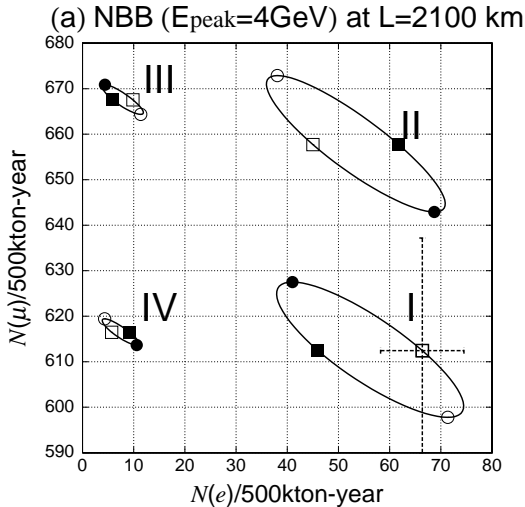


Figure 12. The expected number of mu-like and e-like events for the future T2B experiment with the beam HENBB(4GeV).

dominant $\nu_\mu \rightarrow \nu_\tau$ oscillation mode becomes significant, and their leptonic decay modes have also been counted as background. The contours shown in Fig. 12 are the prediction of the three neutrino model for $\Delta m^2_{\text{ATM}} = 3.5 \times 10^{-3} \text{ eV}^2$, which was the preferred value a few years ago. The results are for 500 kton·year, or for 5 years with the 0.75 MW J-PARC and a 100 kton BAND. They are shown for all the hierarchy cases I, II, III, IV of Fig. 1, where the results for the cases II and IV can be interpreted as the expectation for anti-neutrino oscillation experiments, according to the theorem eq. (11), after the ratio $\sigma_{\text{CC}}(\bar{\nu}_\ell)/\sigma_{\text{CC}}(\nu_\ell) \sim 1/3$ is multiplied.

It is most striking to learn from the figure that the $\nu_\mu \rightarrow \nu_e$ oscillation probability is almost a factor of 7 smaller in the inverted hierarchy (III) than the normal hierarchy (I). On the contrary, the $\bar{\nu}_\mu \rightarrow \bar{\nu}_e$ oscillation is suppressed for the normal hierarchy (IV). This is clearly due to the enhanced matter effects at

high energies, because such significant suppression has not been identified in our previous studies for the T-to-HK project, where the observation of the $\bar{\nu}_\mu \rightarrow \bar{\nu}_e$ events are essential to determine the CP-violating parameter, J_{MNS} or $\sin \delta_{\text{MNS}}$. The two experiments measure approximately the same phase of the oscillation probability, because $L/E = 295 \text{ km}/0.7 \text{ GeV}$ is not far from $2,100 \text{ km}/4 \text{ GeV}$.

This can be understood qualitatively as follows. The oscillation probability $P_{\nu_\mu \rightarrow \nu_e}$ inside of the matter can be expressed as eq. (14c), where the mass squared differences and the mixing matrix are replaced by the corresponding ones $\delta\tilde{m}_{ij}^2$ and $\tilde{U}_{\alpha i}$ according to eq. (23). From eq. (14c), we can tell that the difference in $P_{\nu_\mu \rightarrow \nu_e}$ between the mass hierarchy I and III should come from the difference in the second term proportional to Δ_{12} , which changes the sign between I and III. We find that the mixing matrix terms do not change significantly in the relevant energy region, and the second term contributes constructively for the normal hierarchy (I), whereas destructively for the inverted case (III), as long as $|\tilde{\Delta}_{13}| < \pi$. From Fig. 2, we find that the magnitude of the term $\delta\tilde{m}_{12}^2$ grows rapidly in a few to several GeV region, approaching that of the leading terms of the order δm^2_{ATM} . Although the similar trend is observed for the oscillation at $E_\nu \sim 0.7 \text{ GeV}$ for the T2K and T-to-HK projects, the effects are small enough to be compensated by shifts in the other model parameters, notably $\sin^2 2\theta_{\text{RCT}}$ and δ_{MNS} .

This drastic suppression of $\nu_\mu \rightarrow \nu_e$ oscillation probability for the inverted hierarchy at high energies gives us a powerful tool to determine the neutrino mass hierarchy at very long baseline neutrino oscillation experiments which are capable of detecting electrons. The difference in the predictions of the normal and the inverted hierarchy cases at $\sin^2 2\theta_{\text{RCT}} \sim 0.1$ is so huge that no adjustment of the other model parameters can compensate for it. The Tokai-to-Beijing project with HENBB seems to be an ideal example of such experiments. In Fig. 13, we show the results of simple statistical analysis [11], where we calculated the number of expected events at BAND after 5 years of HENBB at $E_p = 4 \text{ GeV}$ and another 5

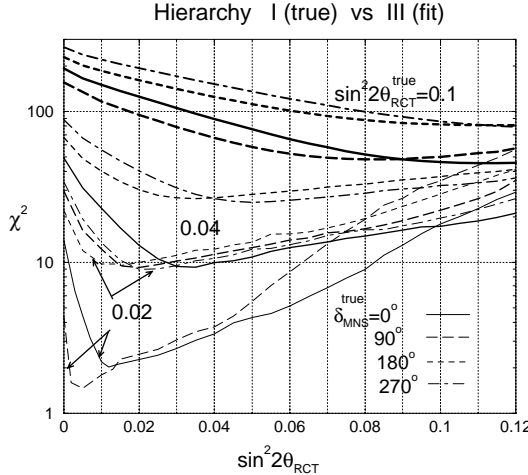


Figure 13. The expected minimum chi-squared of the combined T2K and T2B experiments when the normal hierarchy is realized in the nature while the inverted hierarchy is wrongly assumed in the analysis.

years at 6 GeV for the normal hierarchy and then by analyzing the ‘data’ by assuming the inverted hierarchy. The results of our analysis depend seriously on the assumed value of $\sin^2 2\theta_{\text{RCT}}$, and hence the χ^2_{min} values of our statistical analysis is shown as functions of the $\sin^2 2\theta_{\text{RCT}}$ value in the fit. We examined the cases with the input (‘true’) parameters at $\sin^2 2\theta_{\text{RCT}}^{\text{true}} = 0.1$, 0.04 and 0.02 , for the 4 phase angles, $\delta_{\text{MNS}}^{\text{true}} = 0^\circ, 90^\circ, 180^\circ$ and 270° . It can be seen from the figure that if $\sin^2 2\theta_{\text{RCT}}^{\text{true}} > 0.04$ and the hierarchy is normal (I), then the inverted hierarchy case (III) can be excluded at 3σ level for any values of δ_{MNS} . On the other hand, the generated ‘data’ at $\sin^2 2\theta_{\text{RCT}}^{\text{true}} = 0.02$ for $\delta_{\text{MNS}}^{\text{true}} = 0^\circ$ and 90° can be fitted well within the allowed range of the other model parameters.

We also studied the possibility of constraining the δ_{MNS} parameter in the possible Tokai-to-Beijing project by using the HENBB, but the results we find is not as promising as those from the analysis [20] of the possible Tokai-to-HK project.

The reason is rather simple. If the neutrino mass hierarchy is normal, the oscillation probability for the $\bar{\nu}_\mu \rightarrow \bar{\nu}_e$ is strongly suppressed, and hence we cannot expect much number of events by sending anti-neutrino beams. If the hierarchy is inverted, on the other hand, the $\nu_\mu \rightarrow \nu_e$ oscillation probability is strongly suppressed, and we will need significantly higher power neutrino beams. If the inverted hierarchy is realized in the nature, the Tokai-to-Beijing project with a 4 MW proton accelerator at J-PARC may be necessary. In the Tokai-to-HK project, the use of the low energy neutrino beam helps reducing of the matter effects and a one Mton detector more than compensates for the small cross section at low energies.

In ref. [11], we show the results of our analysis at $L = 1,200\text{km}$ with the HENBB at $E_p = 3\text{ GeV}$ and 5 GeV , and find nearly as promising results as the above Tokai-to-Beijing analysis. If there appears a strong interest in constructing a huge neutrino detector in Korea, this might as well be an appealing option. There, the remnant of the OAB will be studied during the period of the T2K and the planned T-to-HK project, and at a later stage, a new beam-line for the HENBB may be constructed at the J-PARC site to determine the neutrino mass hierarchy.

7. Neutrino Factory at J-PARC

In the final section of my report, I would like to introduce our studies on the possibility of the future very long baseline (VLBL) neutrino oscillation experiments with a neutrino factory at J-PARC and a BAND like 100 kton level detector at a few thousand km away. The possibility of a neutrino factory at J-PARC is being studied in Ref. [26]. For definiteness, we assume a 100 kton-level segmented water-Čerenkov calorimeter detector BAND at $L = 2,100\text{km}$ away from J-PARC, and a neutrino factory at J-PARC which is capable of delivering $10^{21} \mu^+$ or μ^- decays at 10 GeV in one year. We will show that the goals of determining all the neutrino model parameters, including the neutrino mass hierarchy, the sign of $\sin^2 \theta_{\text{ATM}} - 1/2$, and the degeneracy in the CP phase δ_{MNS} , can be reached if such an experiment can be realized.

The physics prospects of VLBL oscillation experiments with a neutrino factory has been studied in the past by assuming that the detector can identify charges [27], and hence the possibility of charge identification at BAND has been investigated [25]. We have tried to show in the report [28] that even if the detector is charge blind, the VLBL experiment will achieve all the physics goals if it is capable of distinguishing the μ -like and e -like events with high confidence level, and if the detector is capable of determining the event energy (the incoming neutrino energy minus the outgoing neutrino energies) at the 10 % level. In the following, we assume that the proposed detector BAND will have such capabilities.

In the neutrino factory, neutrinos are produced from the decay of high energy muons, $\mu^+ \rightarrow \bar{\nu}_\mu \nu_e e^+$ or $\mu^- \rightarrow \nu_\mu \bar{\nu}_e e^-$. Not only the shape and the ratios of the neutrino fluxes but also their overall normalization will be known accurately in the neutrino factory experiments. Assuming the relativistic muons, the $\bar{\nu}_\mu$ and ν_e (ν_μ and $\bar{\nu}_e$) fluxes from $\mu^+(\mu^-)$ beam are expressed as

$$\Phi_{\bar{\nu}_\mu(\nu_\mu)} = \frac{\gamma^2 n_\mu}{\pi L^2} 2y^2[(3 - 2y) \mp P_\mu(1 - 2y)], \quad (44a)$$

$$\Phi_{\nu_e(\bar{\nu}_e)} = \frac{\gamma^2 n_\mu}{\pi L^2} 12y^2[(1 - y) \mp P_\mu(1 - y)], \quad (44b)$$

where $\gamma = E_\nu/m_\mu$, $y = E_\nu/E_\mu$, and P_μ is the average muon polarization, and n_μ is the number of the decaying muons for which we assume 10^{21} per year in the following.

The e -like signal from μ^+ beam, $N_e(\mu^+)$, is given by the sum of e^+ from $\bar{\nu}_\mu \rightarrow \bar{\nu}_e$ appearance and e^- from the $\nu_e \rightarrow \nu_e$ survival mode, whereas the μ -like signal, $N_\mu(\mu^+)$, is the sum of μ^+ from $\bar{\nu}_\mu \rightarrow \bar{\nu}_\mu$ and μ^- from $\nu_e \rightarrow \nu_\mu$;

$$N_e(\mu^+) : (\nu_e \rightarrow \nu_e) + (\bar{\nu}_\mu \rightarrow \bar{\nu}_e), \quad (45a)$$

$$N_\mu(\mu^+) : (\bar{\nu}_\mu \rightarrow \bar{\nu}_\mu) + (\nu_e \rightarrow \nu_\mu). \quad (45b)$$

The signals from the μ^- beam, $N_e(\mu^-)$ and $N_\mu(\mu^-)$, are obtained in the same way:

$$N_e(\mu^-) : (\bar{\nu}_e \rightarrow \bar{\nu}_e) + (\nu_\mu \rightarrow \nu_e), \quad (46a)$$

$$N_\mu(\mu^-) : (\nu_\mu \rightarrow \nu_\mu) + (\bar{\nu}_e \rightarrow \bar{\nu}_\mu). \quad (46b)$$

These signals in the i -th energy bin,

$$\frac{i+1}{10} E_{\mu^\pm} < E_{\text{obs}} < \frac{i+2}{10} E_{\mu^\pm}, \quad (47)$$

are then calculated by ignoring the energy resolution errors, but correcting for the missing neutrino energies in the events where e^\pm and μ^\pm comes from τ^\pm production via the charged currents. In the following analysis we dropped from our analysis low energy events with $E_{\text{obs}} < 2$ GeV.

The results are shown in Fig. 14 for 10^{21} decaying μ^+ (top two figures) and μ^- (bottom two figures) each at 10 GeV. The results for the normal-hierarchy are given in thick lines and those of the inverted hierarchy are in thin lines; the solid, dashed, and dot-dashed lines are for $\sin^2 \theta_{\text{ATM}} = 0.5, 0.35$, and 0.65 , respectively. The other model parameters are chosen as in eq. (39) at $\sin^2 2\theta_{\text{RCT}} = 0.06$ and $\delta_{\text{MNS}} = 0^\circ$.

The contribution from the survival mode dominates the μ -like signal but they vanish at around $E_\nu \simeq 5$ GeV for both $N_\mu(\mu^+)$ and $N_\mu(\mu^-)$, where most of μ neutrinos oscillate into τ neutrinos. Therefore the μ -like events in the surrounding energy bins are sensitive to the $\nu_e \rightarrow \nu_\mu$ or $\bar{\nu}_e \rightarrow \bar{\nu}_\mu$ transition probability.

For instance, in the histogram for $N_\mu(\mu^+)$, we can see significant dependence on the sign of $\sin^2 \theta_{\text{ATM}} - 1/2$, especially around $E_\nu \simeq 5$ GeV. The sensitivity is due to the $\nu_e \rightarrow \nu_\mu$ appearance mode, whose probability is proportional to $\sin^2 \theta_{\text{ATM}} \sin^2 \theta_{\text{RCT}}$, just like the $\nu_\mu \rightarrow \nu_e$ oscillation probability in eq. (14c). In order to resolve the degeneracy in the sign of $\sin^2 \theta_{\text{ATM}} - 1/2$, however, we need to have an independent measurement of $\sin^2 2\theta_{\text{RCT}}$.

We observe from Fig. 14 that $N_e(\mu^+)$ is very insensitive to $\sin^2 \theta_{\text{ATM}} - 1/2$ throughout the energy bins. This is especially so for the normal hierarchy, where the $\bar{\nu}_\mu \rightarrow \bar{\nu}_e$ oscillation is strongly suppressed due to the matter effects, as explained in the previous section, see Fig. 12. Although the suppression is absent for the inverted hierarchy, the contributions from the $\bar{\nu}_\mu \rightarrow \bar{\nu}_e$ transition is still suppressed significantly because of the small anti-neutrino cross sections on the matter target. It is therefore envisaged that the measurement of $N_e(\mu^+)$ will give us the desired independent measurement of $\sin^2 2\theta_{\text{RCT}}$ because it is dominated by the $\nu_e \rightarrow \nu_e$ survival mode, especially when the mass hierarchy is normal. Therefore, the neutrino

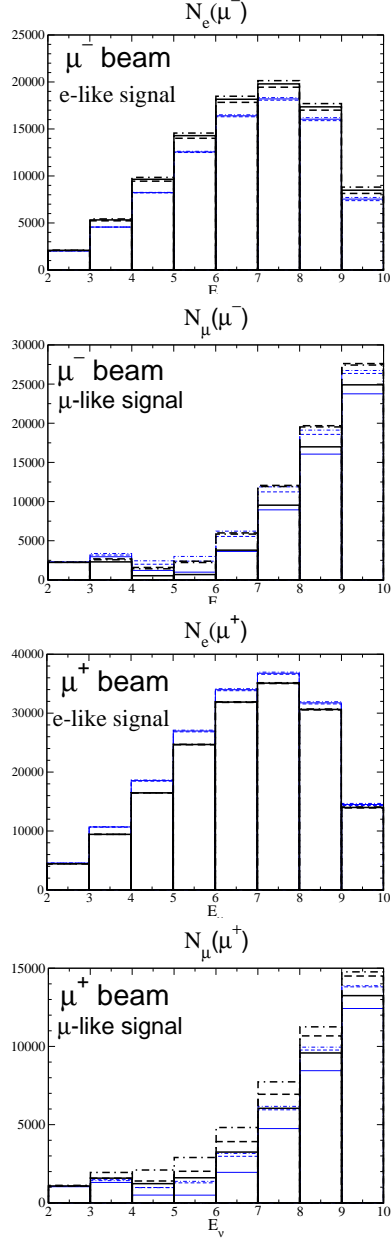


Figure 14. Number of e - and μ -like signals for 10^{21} decaying μ^+ (top two) and μ^- (bottom two) each at 10 GeV. Thick lines are for the normal hierarchy, and thin lines are for inverted; $\sin^2 \theta_{\text{ATM}} = 0.5$ (solid lines), 0.35 (dashed lines), and 0.65 (dot-dashed lines).

factory VLBL experiments with a detector capable for distinguishing e^\pm events from μ^\pm can give us a precise measurement of $\sin^2 2\theta_{\text{RCT}}$ just like the next generation reactor experiments [22,23]. In addition, the presence of the enhanced large matter effects for the $\nu_\mu \leftrightarrow \nu_e$ and $\bar{\nu}_\mu \leftrightarrow \bar{\nu}_e$ make the inter-dependences of the four observables in Fig. 14 very different between the normal and the inverted hierarchies. We also find that the results depend rather significantly on the input δ_{MNS} value if $\sin^2 2\theta_{\text{RCT}}$ is not too small. Because the energy dependence of the signal can be studied in the wide range of L/E at VLBL experiments with a neutrino factory, the degeneracy between $\delta_{\text{MNS}} = 0^\circ$ and 180° can also be resolved [28].

We performed a χ^2 analysis similar to the ones we performed for the Tokai-to-HK [20] and the Tokai-to-Beijing [11] projects, in order to study these questions quantitatively. The additional assumption that we make for the detector is that it is capable of measuring the event energy calorimetrically, with the accuracy which makes the error of our analysis based on the 1 GeV bin histogram small. The energy threshold of $E_\nu > 2$ GeV has been introduced to avoid numerical sensitivity to the binning due to rapid oscillation. Our analysis is hence performed for 8 bins between $E_\nu = 2$ GeV and 10 GeV.

Because the expected number of events is huge for the above experimental set up, a few tenths of sounds of events for each bin, as can be seen from Fig. 14, we introduced the following systematic uncertainties in the analysis:

- 2 % error each in the detection efficiency of e -like and μ -like events
- 2 % error each in the CC cross section of neutrinos and anti-neutrinos

Here we assumed that the errors in the detection efficiencies are independent for e -like and μ -like events, and also the errors in the ν and $\bar{\nu}$ cross sections are independent. On the other hand we assume that the errors for ν_e and ν_μ cross sections are common (100 % correlated), as well as for their anti-neutrino counterparts. Since the experiments will be performed more than a decade

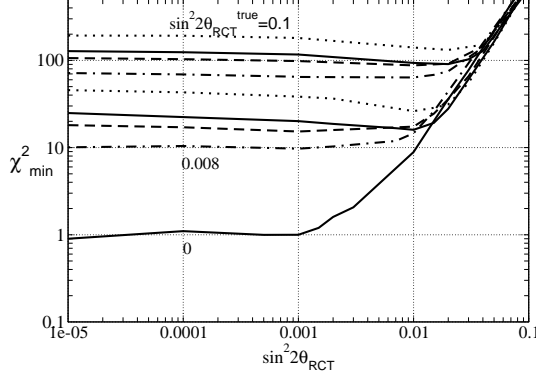


Figure 15. χ^2_{\min} as a function of the fitting parameter $\sin^2 2\theta_{\text{RCT}}$ when the input events are generated for the normal hierarchy (I) and the analysis is done by assuming the inverted hierarchy (III). The input data are calculated for $\sin^2 \theta_{\text{ATM}}^{\text{true}} = 0.5$ at $\sin^2 2\theta_{\text{RCT}}^{\text{true}} = 0.1, 0.008$ and 0. The four curves are for $\delta_{\text{MNS}} = 0^\circ$ (solid), 90° (dotted), 180° (dash) and 270° (dot-dash).

in the future, it is possible that the systematic errors can be reduced even further. In ref. [28], we also show the results when the above systematic errors are set to zero.

We show in Fig. 15 the χ^2_{\min} value as a function of $\sin^2 2\theta_{\text{RCT}}$, when the ‘data’ are generated by assuming the normal hierarchy, while the analysis is done by assuming the inverted hierarchy. We show our results for $\sin^2 2\theta_{\text{RCT}}^{\text{true}} = 0.1, 0.008$, and 0, and for the four CP violating phase angles; $\delta_{\text{MNS}} = 0^\circ, 90^\circ, 180^\circ$ and 270° . The results show that we can distinguish between the normal and the inverted mass hierarchy at 3- σ level, if $\sin^2 2\theta_{\text{RCT}}^{\text{true}} \gtrsim 0.008$. At small $\sin^2 2\theta_{\text{RCT}}$, we find that the contributions of the transition modes become negligible, but the e -like signals from both μ^+ and μ^- beams are useful in determine the hierarchy. This is because the disappearance probability is suppressed for the $\bar{\nu}_e \rightarrow \bar{\nu}_e$ transition in the normal hierarchy, whereas that of $\nu_e \rightarrow \nu_e$ is suppressed in the inverted hierarchy. However, the differences of the e -like signals between

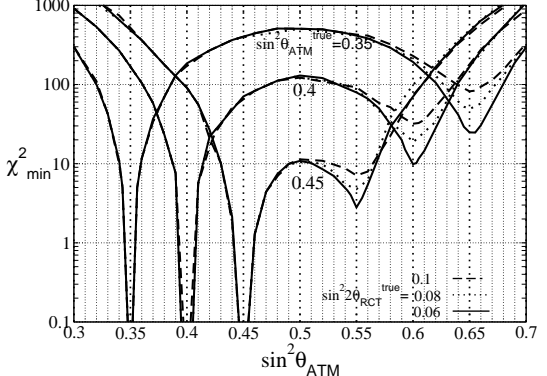


Figure 16. χ^2_{\min} as a function of the fitting parameter $\sin^2 \theta_{\text{ATM}}$. The input data of the events are calculated for $\sin^2 \theta_{\text{ATM}}^{\text{true}} = 0.35, 0.4$, and 0.45 with $\sin^2 2\theta_{\text{RCT}}^{\text{true}} = 0.06$ (solid lines), 0.08 (dotted lines) and 0.1 (dashed lines) and $\delta_{\text{MNS}}^{\text{true}} = 0^\circ$. The other input values are the same as in eq. (39).

the normal and the inverted hierarchy reduces to $\sim 1\%$ when $\sin^2 2\theta_{\text{RCT}} = 0.004$, and the sensitivity is limited by our knowledge on the ratio $\sigma_{\text{CC}}(\bar{\nu}_e)/\sigma_{\text{CC}}(\nu_e)$.

We show in Fig. 16 the χ^2_{\min} as a function of $\sin^2 \theta_{\text{ATM}}$. The input ‘data’ are calculated for $\sin^2 \theta_{\text{ATM}}^{\text{true}} = 0.35, 0.4$, and 0.45 for three values of $\sin^2 2\theta_{\text{RCT}}^{\text{true}} = 0.1$ (dashed lines), 0.08 (dotted lines) and 0.06 (solid lines), and for $\delta_{\text{MNS}}^{\text{true}} = 0^\circ$ with the normal hierarchy. The values of the other parameters are taken as in eq. (39). The χ^2_{\min} function is found by varying the fitting parameters within the normal hierarchy. We see that each χ^2_{\min} has two dips at the $\sin^2 \theta_{\text{ATM}}$ values which give the same $\sin^2 2\theta_{\text{ATM}}$. The results show that we can resolve the degeneracy at the 3- σ level when $\sin^2 \theta_{\text{ATM}} = 0.35$ ($\sin^2 2\theta_{\text{ATM}} = 0.91$) or 0.4 ($\sin^2 2\theta_{\text{ATM}} = 0.96$) for all the three $\sin^2 2\theta_{\text{RCT}}$ values considered ($\sin^2 2\theta_{\text{RCT}}^{\text{true}} \geq 0.06$), but that $\sin^2 \theta_{\text{ATM}}^{\text{true}} = 0.45$ ($\sin^2 2\theta_{\text{ATM}}^{\text{true}} = 0.99$) can be resolved from $\sin^2 \theta_{\text{ATM}} = 0.55$ at 3- σ only if $\sin^2 2\theta_{\text{RCT}}^{\text{true}} \gtrsim 0.1$.

In Fig. 17, we show the allowed regions in the

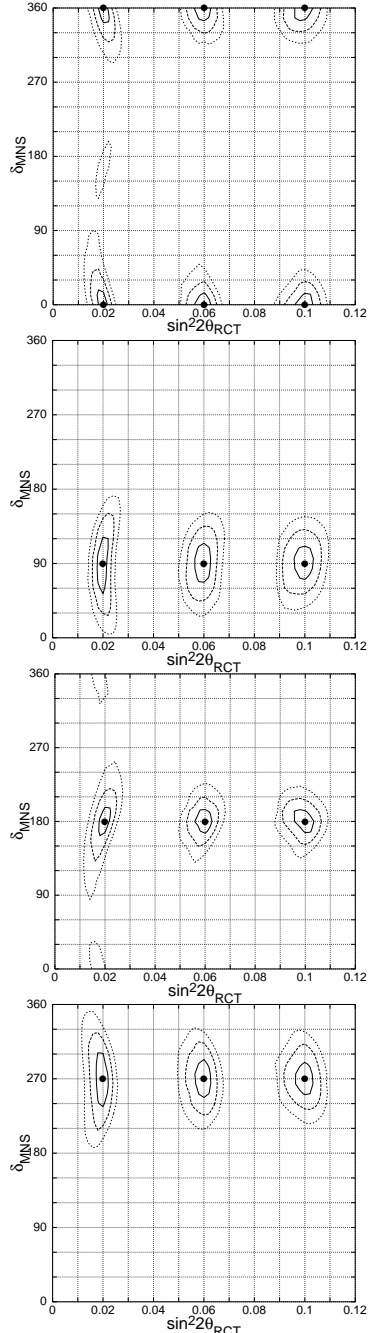


Figure 17. Allowed regions in the plane of $\sin^2 2\theta_{\text{RCT}}$ and δ_{MNS} for $\sin^2 2\theta_{\text{RCT}}^{\text{true}} = 0.02, 0.06$ and 0.1 , for $\delta_{\text{MNS}}^{\text{true}} = 0^\circ, 90^\circ, 180^\circ$ and 270° .

plane of $\sin^2 2\theta_{\text{RCT}}$ and δ_{MNS} for $\sin^2 2\theta_{\text{RCT}}^{\text{true}} = 0.02, 0.06$, and 0.1 and $\delta_{\text{MNS}}^{\text{true}} = 0^\circ$ (top), 90° (second), 180° (third), and 270° (bottom) in the normal hierarchy. In each figure, the input parameter points are shown by solid-circles. The normal hierarchy is assumed in the fitting. The regions where $\chi^2_{\text{min}} < 1, 4$, and 9 are depicted by solid, dashed, and dotted boundaries, respectively.

The figures for $\delta_{\text{MNS}}^{\text{true}} = 90^\circ$ and $\delta_{\text{MNS}}^{\text{true}} = 270^\circ$ show that the CP phase δ_{MNS} can be constrained locally around the ‘true’ points for all the input $\sin^2 2\theta_{\text{RCT}}$ values. We can hence establish CP violation in the leptonic sector, and discriminate the maximal CP violation, $\delta_{\text{MNS}}^{\text{true}} = 90^\circ$ or 270° , from the CP conserving cases of $\delta_{\text{MNS}}^{\text{true}} = 0^\circ$ or 180° at the 3σ level if $\sin^2 2\theta_{\text{RCT}}^{\text{true}} \gtrsim 0.02$. The discrimination between $\delta_{\text{MNS}}^{\text{true}} = 0^\circ$ and 180° is also possible at the same level, but for the small $4 < \chi^2_{\text{min}} < 9$ island at $\sin^2 2\theta_{\text{RCT}}^{\text{true}} = 0.02$.

The above results for CP violation are comparable to those of Tokai-to-HK studies shown in Fig. 5. The sensitivity in this analysis, with the neutrino factory and a charge-blind detector, is based essentially on the T violating difference between $P_{\nu_e \rightarrow \nu_\mu}$ and $P_{\nu_\mu \rightarrow \nu_e}$. Because the matter effects enhance both of these transitions whereas suppress strongly the transitions $\bar{\nu}_\mu \rightarrow \bar{\nu}_e$ and $\bar{\nu}_e \rightarrow \bar{\nu}_\mu$, $N_\mu(\mu^+)$ is sensitive to $P_{\nu_e \rightarrow \nu_\mu}$ and $N_e(\mu^-)$ is sensitive to $P_{\nu_\mu \rightarrow \nu_e}$. Therefore, the above results are obtained only when the neutrino mass hierarchy is normal. A significantly less accurate results are expected if the mass hierarchy turns out to be inverted, because the enhanced transition modes appear for the anti-neutrinos whose cross sections on the matter is a factor of 3 smaller than the neutrino cross sections.

Summing up, the following results are expected for a VLBL experiment with a neutrino factory which delivers 10^{21} decaying μ^+ and μ^- at 10 GeV and a 100 kton detector which is placed 2,100 km away and is capable of measuring the event energy and distinguishing e^\pm from μ^\pm , but not their charges: The neutrino mass hierarchy can be determined if $\sin^2 2\theta_{\text{RCT}} \gtrsim 0.008$, the degeneracy in $\sin^2 \theta_{\text{ATM}}$ can be resolved for $\sin^2 2\theta_{\text{ATM}} = 0.96$ if $\sin^2 2\theta_{\text{RCT}} \gtrsim 0.06$, and the CP-violating phase δ_{MNS} can be uniquely con-

strained for $\sin^2 2\theta_{\text{RCT}} \gtrsim 0.02$ if its true value is around 90° or 270° , while it can be constrained for $\sin^2 2\theta_{\text{RCT}} \gtrsim 0.04$ if its true value is around 0° or 180° , all at the 3σ level.

Acknowledgments

Let me first thank my collaborators, Mayumi Aoki, Naotoshi Okamura, and Ken-ichi Senda. All the results presented in this report are based on the works done or being done with them. I also learned a lot from stimulating discussions with our colleagues, Y. Hayato, T. Kobayashi, T. Nakaya and K. Nishikawa.

REFERENCES

1. The LSND Collaboration (A. Aguilar *et al.*), Phys. Rev. **D64**, 112007 (2001).
2. The Super-Kamiokande Collaboration (Y. Fukuda *et al.*), Phys. Lett. **B433**, 9 (1998); Phys. Rev. Lett. **81**, 1562 (1998).
3. The K2K collaboration (M.H. Ahn *et al.*), Phys. Rev. Lett. **90**, 041801 (2003), hep-ex/0212007.
4. The Super-Kamiokande Collaboration (Y. Ashie *et al.*), hep-ex/0404034.
5. B. Kayser, in Review of Particle Physics, Phys. Lett. **B592** (1) 2004, pp. 145–153, and references therein.
6. The KamLAND Collaboration (T. Araki *et al.*), hep-ex/0406035.
7. The CHOOZ Collaboration (M. Apollonio *et al.*), Eur. Phys. J. **C27**, 331 (2003), hep-ex/0301017.
8. M.H. Shaevitz, for the MiniBooNE Collaboration, hep-ex/0407027.
9. Z. Maki, M. Nakagawa and S. Sakata, Prog. Theor. Phys. **28**, 870 (1962).
10. K. Hagiwara and N. Okamura, Nucl. Phys. **B548**, 60 (1999).
11. M. Aoki, K. Hagiwara, Y. Hayato, T. Kobayashi, T. Nakaya, K. Nishikawa, and N. Okamura, Phys. Rev. **D67**, 093004 (2003).
12. K. Hagiwara, lecture at “*Topical Seminar on Frontier of Particle Physics 2002: Neutrinos and Cosmology*”, Beijing, August 20-25, 2002. <http://bes.ihep.ac.cn/conference/particle/2002/>
13. L. Wolfenstein, Phys. Rev. **D17**, 2369 (1978); R.R. Lewis, *ibid.* **21**, 663 (1980); V. Barger, S. Pakvasa, R.J.N. Phillips and K. Whisnant, *ibid.* **22**, 2718 (1980).
14. S.P. Mikheyev and A.Yu. Smirnov, Yad. Fiz. **42**, 1441 (1985), [Sov.J.Nucl.Phys. **42**, 913 (1986)]; Nuovo Cimento **C9**, 17 (1986).
15. H. Yokomakura, K. Kimura and A. Taka-mura, Phys. Lett. **B544**, 286 (2002).
16. The MINOS Collaboration home page, <http://www-numi.fnal.gov/>.
17. Y. Itow *et al.* (JHF-Kamioka neutrino Project), hep-ex/0106019; see also the JHF Neutrino Working Group’s home page, <http://neutrino.kek.jp/jhfnu/>.
18. J-PARC home page, <http://j-parc.jp/>.
19. See *e.g.* , T. Kobayashi, presented at NP02, Kyoto, Sept. 2002.
20. M. Aoki, K. Hagiwara, and N. Okamura, Phys. Lett. **B554**, 121 (2003).
21. M. Aoki, K. Hagiwara, and N. Okamura, in preparation.
22. The Double-CHOOZ Collaboration, hep-ex/0405032
23. The KASKA Collaboration, hep-ex/0407016
24. K. Hagiwara, N. Okamura, and K. Senda, in preparation.
25. Y.F. Wang, hep-ex/0010081; H. Chen, *et al.*, hep-ph/0104266; Y.F. Wang, *et al.*, Phys. Rev. **D65**, 073021 (2002).
26. See *e.g.* , Y. Kuno *et al.* <http://www-prism.kek.jp/nufactj/index.html>.
27. A. Cervera *et al.*, Nucl. Phys. **B579**, 17 (2000); Erratum-*ibid.* Nucl. Phys. **B593**, 731 (2001); Nucl. Instrum. Meth. **A472**, 403 (2000); A. Donini, D. Meloni, P. Migliozzi, Nucl. Phys. **B646**, 321 (2002); V. Barger, S. Geer, R. Raja, K. Whisnant, Phys. Lett. **B485**, 379 (2000) V. Barger, D. Marfatia, K. Whisnant, Phys. Rev. **D65**, 073023 (2002).
28. M. Aoki, K. Hagiwara and N. Okamura, hep-ph/0311324; revised manuscript in preparation.